J Nanopart Res (2011) 13:511–524
DOI 10.1007/s11051-010-0081-5

RESEARCH PAPER

Generation and characterization of stable, highly concentrated titanium dioxide nanoparticle aerosols for rodent inhalation studies

Wolfgang G. Kreyling · Pratim Biswas · Maria E. Messing · Neil Gibson · Marianne Geiser · Alexander Wenk · Manoranjan Sahu · Knut Deppert · Izabela Cydzik · Christoph Wigge · Otmar Schmid · Manuela Semmler-Behnke

Received: 8 May 2010 / Accepted: 1 September 2010 / Published online: 18 September 2010

Abstract The intensive use of nano-sized titanium dioxide (TiO_2) particles in many different applications necessitates studies on their risk assessment as there are still open questions on their safe handling and utilization. For reliable risk assessment, the interaction of TiO_2 nanoparticles (NP) with biological systems ideally needs to be investigated using physico-chemically uniform and well-characterized NP. In this article, we describe the reproducible production of TiO_2 NP aerosols using spark ignition technology. Because currently no data are available on inhaled NP in the 10–50 nm diameter range, the emphasis was to generate NP as small as 20 nm for inhalation studies in rodents. For anticipated in vivo dosimetry analyses, TiO_2 NP were radiolabeled with ^{48}V by proton irradiation of the titanium electrodes of the spark generator. The dissolution rate of the ^{48}V label was about 1% within the first day. The highly concentrated, polydisperse TiO_2 NP aerosol ($3–6 \times 10^6$ cm^{-3}) proved to be constant over several hours in terms of its count median mobility diameter, its geometric standard deviation, and number concentration. Extensive characterization of NP chemical composition, physical structure, morphology, and specific surface area was performed. The originally generated amorphous TiO_2 NP were converted into crystalline anatase TiO_2 NP by thermal annealing at 950 °C. Both crystalline and amorphous 20-nm TiO_2 NP were chain agglomerated/aggregated, consisting of primary particles in the range of 5 nm. Disintegration of the deposited TiO_2 NP in lung tissue was not detectable within 24 h.

Keywords Titanium dioxide · Anatase · Amorphous TiO_2 · Spark ignition · Chain aggregate/agglomerate · Nanoparticle generation · Transmission electron microscopy · Elemental microanalysis · Electron tomography · Environmental, health and safety (EHS)

W. G. Kreyling (✉) · A. Wenk · O. Schmid · M. Semmler-Behnke
Comprehensive Pneumology Center, Institute of Lung Biology and Disease and Focus Network Nanoparticles and Health, Helmholtz Zentrum München—Research Center for Environmental Health, 85764 Neuherberg, Munich, Germany
e-mail: kreyling@helmholtz-muenchen.de
URL: http://www.helmholtz-muenchen.de/en/research/en/ilbd/ilbd-home/index.html

P. Biswas · M. Sahu
Department of Energy, Environmental and Chemical Engineering, Washington University in St. Louis, Campus Box 1180, St. Louis, MO 63130, USA

M. E. Messing · K. Deppert
Solid State Physics, Lund University, Box 118, SE-22 100 Lund, Sweden

N. Gibson · I. Cydzik
Institute for Health and Consumer Protection, Joint Research Centre of the European Commission, via E. Fermi 2749, 21020 Ispra, VA, Italy

M. Geiser · C. Wigge
Institute of Anatomy, University of Bern, Baltzerstrasse 2, 3000 Bern 9, Switzerland

Introduction

Nanoscaled, pigment-grade titanium dioxide (TiO_2) is widely used in many fields of industrial technology, consumer products, science, and medicine (Zhang et al. 2001; Chen and Mao 2007; Almquist et al. 2003; Nohynek et al. 2008; Li et al. 2008; Rehman et al. 2009; Barnard 2010). However, the fraction of nanoscaled TiO_2 is most often not identified. Yet it appears plausible that pigment-grade TiO_2 contains a fraction of nanoscale TiO_2 with particulate structures less than 100 nm in size. In industrial products such as paints, plastics, papers, inks, food colorants, and toothpastes TiO_2 provides whiteness and opacity. In cosmetic and skin care products, particularly in sun cream, it protects the skin from UV light. In medicine and pharmacy, it is used in prostheses and as filler and coating of medicaments. Particulate TiO_2 comes in many forms; besides the two dominant crystalline structures, anatase and rutile and mixtures thereof, it may have an amorphous structure. Furthermore, there are many options for surface coatings and other surface modifications (Zhang et al. 2001; Chen and Mao 2007; Almquist et al. 2003; Nohynek et al. 2008; Li et al. 2008). In addition, particulate TiO_2 may well be used in mixtures of other pigment or nanoscaled materials.

Although TiO_2 is chemically not very reactive, TiO_2 NP have been shown to cause adverse health effects, such as respiratory tract cancer in rats (Heinrich et al. 1995; Borm et al. 2004; Dankovic et al. 2007). Recently, Jiang et al. (2008) reported the complex relationship between NP size (from 4 to 195 nm) and crystalline structure of TiO_2 NP, and their ability to induce reactive oxygen species (ROS) and subsequent inflammatory responses. However, epidemiologic studies conducted on workers exposed to pigment-grade TiO_2 have not found an association between occupational exposure to TiO_2 and increased risk for lung cancer (Boffetta et al. 2004; Fryzek et al. 2003). Thus far, there are very few studies on oral uptake of particulate TiO_2. Lomer et al. (2004) reported an average daily uptake of 4.5 mg of manufactured TiO_2 in a survey of more than 600 individuals. In addition, only limited data are there on uptake and biokinetics of particulate TiO_2. According to the study by Jani et al. (1994) in healthy rats, up to 5% of the oral uptake of engineered TiO_2 leads to absorption and distribution in the entire body. If this fraction is applied to humans, then a continuous daily dose of several hundreds of microgram of engineered TiO_2 is expected to be absorbed and distributed in the body of each individual of the general population every day, with nanoscale TiO_2 particles most likely to be absorbed. Hence, a thorough study on the fate of nanoscale TiO_2 particles in the body is needed.

In this article, we focus on the generation and characterization of well-defined TiO_2 NP for use in inhalation studies since developing the science and technology of NP production for toxicology studies is essential in its own right to allow us to understand and minimize the potential health impacts. With respect to the investigation of health impacts, the following questions need to be addressed:

(1) distribution and transport of particles within the respiratory tract;
(2) their subsequent biokinetic fate across the air–blood barrier into circulation and accumulation in organs and tissues of the entire organism;
(3) toxicological responses of the various tissues in the lungs and the entire organism.

Transmission electron microscopic (TEM) analysis of NP at the individual particle level in tissues is important as it provides information about which cells and intracellular components are the targets of (inhaled) particles. Such investigations have been reported already for amorphous TiO_2 NP aerosol generated with the system described in this article (Kapp et al. 2004; Geiser et al. 2005, 2008). These analyses contribute to the understanding of underlying mechanisms and modes of actions that may eventually lead to adverse health effects. Prerequisites for such studies include adequate particle application and tissue preservation, representative tissue, and particle sampling for quantitative analysis (unbiased stereology), as well as unambiguous particle identification (Geiser and Kreyling 2010).

Materials and methods

Generation of TiO_2 NP using spark ignition technology for online inhalation studies

Using a spark aerosol generator (GFG100, Palas, Karlsruhe, Germany), sparks were ignited by a high-voltage discharge between two adjacent titanium rod

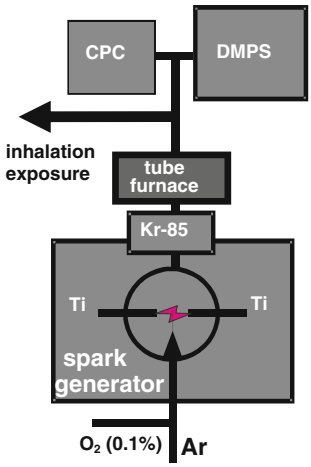

Fig. 1 Schematics of TiO_2 NP generation and online size and concentration analysis

electrodes in an argon (Ar) gas stream of 3 L min^{-1} with 0.1 vol% of oxygen (O_2), as shown in Fig. 1. In this spark ignition process, a tiny amount of titanium of the electrode surface evaporates and condenses very quickly forming primary particles. By altering the frequency of the spark ignition, the resulting mass output and hence the coagulation-driven size distribution of the chain-agglomerated/aggregated NP can be varied. Because of the O_2 content in the gas stream, these particles have already become composed of TiO_2. These primary particles appear at very high concentrations ($\gg 10^8$ cm^{-3}), such that rapid coagulation occurs during the cooling. According to the initial high spark temperature, aggregates with firm chemical bonds will be formed. During further cooling, agglomerates will be formed by weak physical, e.g., van der Waal forces. The highly charged aerosol was quasi-neutralized by an inline radioactive ^{85}Kr source about 10 cm^3 downstream of the spark generation chamber. Further coagulation was stopped by diluting the aerosol with oxygen and nitrogen to obtain an oxygen concentration of 20–25% at a flow rate of typically 10 L min^{-1}. The oxygen/nitrogen mixture was humidified by controlled diffusion of water molecules through a semi-permeable tube to achieve a final relative humidity of the aerosol that is modifiable between 50 and 80%. The aerosol was fed through a rodent inhalation apparatus maintained with an absolute filter and pump unit to adjust the aerosol pressure to be in the range between 20 and 40 Pa below the laboratory pressure. Using this system, a physiological aerosol is provided to the animals for inhalation within 5 s of the initial particle formation.

Various alternative methods exist for the generation of TiO_2 NP aerosols that provide higher mass output rates. However, this is either at the expense of larger particle size due to rapid coagulation, or of higher flow rates which are not desirable, since rodents (rats) do not inhale more than about 0.2 L min^{-1}. Our technique provides the highest number concentration theoretically possible ($3–6 \times 10^6$ cm^{-3}) limited only by unavoidable rapid coagulation, and is ideally suited to rodent inhalation studies. The system is also more suitable than other aerosol techniques for labeling studies (see below) due to the lower amount of radioactive material associated with the limited mass output rate.

^{48}V radiolabeling of TiO_2 NP

Radiolabeling of TiO_2 with ^{48}V has been described earlier (Lekki et al. 2007). The pure cylindrical titanium electrodes (diameter 3 mm; length 5 mm) were proton irradiated in a cyclotron (ZAG, Karlsruhe, Germany) causing a nuclear transformation of non-radioactive ^{48}Ti atoms into radioactive ^{48}V atoms, Fig. 2. The proton beam was directed toward one of the circular tips of both electrodes, at a low

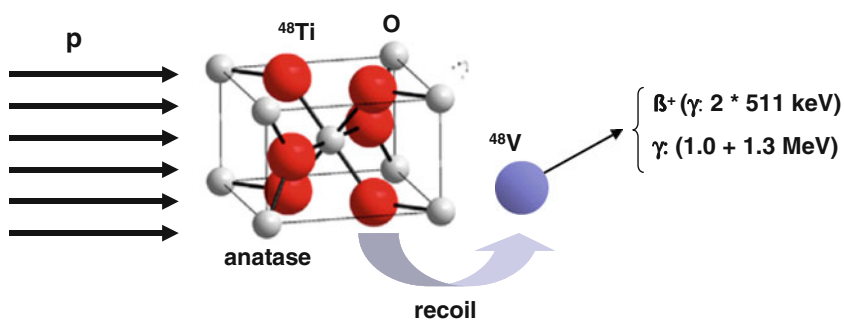

Fig. 2 Schematics of proton irradiation of titanium

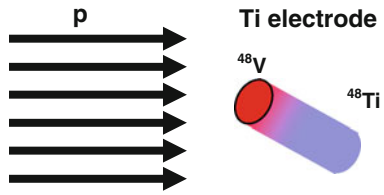

Fig. 3 Proton irradiation of a titanium electrode at a low angle of incidence to one of the circular surfaces

angle of incidence to the surface. Owing to the chosen beam energy, and to beam energy loss in the titanium, the nuclear (p, n) reaction occurred preferentially very near the surface of the electrodes, Fig. 3. Thus, the total ^{48}V radioactivity of 85 MBq per electrode was accumulated in the first few milligram of each tip. The radioactive ^{48}V isotope decays by electron capture and positron emission with major gamma energies at 0.99 and 1.3 MeV; its decay half-life is 15.98 days.

In the case of ^{48}V radiolabeling using irradiated Ti electrodes (see below), thermal treatment of the aerosol was introduced downstream of the ^{85}Kr aerosol neutralizer before the addition of oxygen and nitrogen using a tube furnace at 950 °C for the firm integration of the ^{48}V-atoms into the matrix of the NP aggregates/agglomerates, see Fig. 1.

Aerosol characterization

Size distribution and aerosol concentration were continuously measured online using a condensation particle counter (CPC 3022, TSI, Aachen, Germany) and a differential mobility particle size spectrometer (DMPS consisting of a model 3071 differential mobility analyzer and a model 3010 CPC, TSI, Aachen, Germany). All aerosol lines were made of metal, properly grounded to avoid potential losses due to NP charge. In addition, the aerosol analysis of size and concentration was performed at the same point after generation—as it entered the inhalation apparatus—to ensure correct analysis of the aerosol dynamics at inhalation. This was achieved by adjusting the aerosol residence time by optimizing the volume of the aerosol line to the aerosol instruments in accordance with their flow rates.

The spark generator was usually run at 100–150-Hz spark frequency resulting in NP aerosols with a median mobility diameter of 20–25 nm. Owing to the additional O_2 flow into the spark chamber for titanium oxidization during the generation process, O_3 concentration was monitored at 5-min intervals during several 2-h aerosol production experiments using an ozone monitor (O341M, Environment SA, Poissy, France).

TiO_2 NP morphology and chemical analysis

An electrostatic precipitator (ESP) (3089 TSI, Aachen, Germany) was connected to the spark ignition aerosol generation system to deposit TiO_2 NP for TEM analysis. As-generated (without heat treatment) particles as well as particles treated at 950 °C were directly deposited onto lacey carbon film copper TEM grids placed inside the ESP. A high-resolution TEM (HRTEM, JEOL 3000F, Tachikawa, Japan), equipped with a field emission gun, an X-ray energy dispersive spectrometer (XEDS, Inca, Oxford Instruments, Oxford, UK), and Gatan Imaging Filter (2 × 2 k), operated at 300 kV was used for morphological and chemical investigations of TiO_2 NP.

For chemical composition, XEDS and Electron Energy Loss Spectrometry (EELS) measurements were performed.

Specific surface area analysis of TiO_2 NP

The specific surface area of a 15-mg TiO_2 NP sample collected during 8-h day-shifts over 2 weeks of aerosol production and filter sampling was determined using the BET isotherm (Autosorb-1, Quantachrome Instruments, Florida, USA) by nitrogen adsorption at 77 K. Usually, BET analysis requires a total particle powder surface area of 10 m^2.

TiO_2 NP crystallinity

TiO_2 aerosol was generated and collected on Teflon filters over several days. During the entire production, the aerosol concentration and size distribution were monitored. Production was terminated when a total of about 15 mg of TiO_2 NP was carefully removed from the filters and then transferred into a test tube. This was done for TiO_2 aerosols both with and without thermal treatment to obtain crystalline and amorphous TiO_2 NP, respectively. X-ray diffractometry (XRD) was used for the characterization of crystallinity and

crystal phase of the 15-mg TiO_2 NP sample using a D-MAX/A9 diffractometer (Rigaku, Tokyo, Japan) with copper $K\alpha$ radiation ($\lambda = 1.5418$ Å).

In a second attempt to characterize the crystalline structure of the TiO_2 NP, a small quantity was deposited onto a silicon wafer over an area of several square millimeters by electrostatic point-to-plane precipitation (Intox, Albuquerque, USA). A TiO_2 NP aerosol sample flow of 0.5 L min^{-1} was quantitatively precipitated by a corona current of 2 mA at 3.5 kV between a needle tip and the electrically grounded wafer perpendicular to the aerosol flow; the sampling time was 2 h. The resulting layer was estimated to be a few micrometers thick. This was then examined by glancing-angle XRD (GAXRD), a diffraction technique that is highly surface sensitive, and therefore suitable for analyzing such small quantities of deposited material. The GAXRD system employs a copper $K\alpha$ source and a laser alignment system that ensures accurate control of the incident beam angle and positioning of the sample in the finely collimated incident beam. GAXRD is a non-focusing geometry with a Soller slit being used in the diffracted beam for definition of the angle of the diffracted radiation. The instrumental resolution is of the order of 0.2° (depending on incident beam slit width).

In vitro leaching of the radiolabel ^{48}V from the TiO_2 NP

Aerosols of ^{48}V-TiO_2 NP were collected on an absolute filter and measured with gamma-spectrometry. Subsequently, the filter was mounted in a filter holder with a maximum infusion volume of 200 mL. A volume of 50-mL distilled water was added and after 5 min, 1 h, 24 h, and 3 days, the water was pressed through the filter by compressed air (1.5 bar) and the ^{48}V activity in the filtrate was measured.

TEM analysis of TiO_2 NP in tissue samples: morphological characterization and elemental microanalysis

When studying any particle in biological specimens at the ultrastructural level, unambiguous particle identification is absolutely required. The morphology of the particles has to be known. The first step is to establish the morphology of the aerosol to be inhaled. For this purpose, aerosol-particles collected directly on formvar-coated copper TEM grids using electrostatic precipitation are analyzed, as well as ultrathin sections of aerosol particles collected on filters that are embedded in Epon. These two methods are technically simple, can be performed using any conventional TEM, and can be used to adequately establish the morphology of the aerosol particles and their section profiles.

A technically more challenging method for unambiguous ultrastructural analysis of nanoparticles (NP) in all the three spatial dimensions is electron tomography. 3D structural information of NP and the surrounding tissue is obtained by reconstructing the projections acquired from a multiangular tilt series (Baumeister 2002). The 3D morphology of NP is of special interest because conventional TEM can only produce projections of the NP. We performed electron tomography on untreated, unembedded TiO_2 NP collected from the aerosol on formvar-coated TEM grids directly from the aerosol using a Tecnai F20 field emission TEM (FEI Company, Eindhoven, Netherlands) operating at 200 kV. Typical tilt series were acquired at a magnification of 80,000× covering an angular range between −40 and 40° (with an increment of 2°) and a defocus of −2.66 µm. The pixel size in the tomograms was 0.26 nm. Semi-manual alignment and reconstruction were performed using the FEI software package (Inspect 3D, Amira, FEI Company, Eindhoven Netherlands), while for image processing the ImageJ software, equipped with the volume viewer plugin was used.

Unambiguous identification of TiO_2 NP in ultrathin tissue sections requires not only the morphological identification of the particles by their section profile, but also their elemental microanalysis by Energy Filtering TEM (EFTEM), EELS, and related methods, because there are other structures in the ultrathin tissue section resembling the NP morphologically ("false positives"). In experiments where rats inhaled unlabeled and non-heat-treated aerosols of TiO_2 NP generated by spark ignition as described in this article and lungs were chemically fixed and prepared for ultrastructural analysis either immediately or 24 h after aerosol inhalation, we have adapted three high-resolution and high-sensitivity methods for elemental analysis of TiO_2 NP in ultrathin sections using a LEO 912 (Zeiss, Oberkochen, Germany) microscope (Kapp et al. 2004; Geiser et al. 2005, 2008). We routinely use

electron spectroscopic imaging (ESI), where images are taken at a defined energy loss. Elemental (titanium) mapping is achieved with the three-window method. The background windows are set at $\Delta E = 390$ eV and $\Delta E = 440$ eV, respectively, the titanium-specific window at $\Delta E = 464$ eV ($L_{2,3}$ edge of titanium); the acceleration voltage is 120 kV, and the energy selection slit width is 10 eV. Bright-field and structure-sensitive images (recorded at 0 eV) as well as element-specific contrast for titanium are obtained by digital acquisition (iTEM, Olympus Soft Imaging Solutions GmbH, Münster, Germany). ESI images have reversed contrast as only inelastically scattered electrons are used with an energy loss producing a dark field image.

Results

Generation of TiO_2 NP using spark ignition technology for online inhalation studies

For TiO_2 NP aerosol generation, minimal oxygen was added into the spark chamber to produce NP consisting of TiO_2 and minimize O_3 in the aerosol which would irritate the airways of the exposed rodents. An O_2 flow rate of 0.1% of the Ar flow rate (3 L min^{-1}) was chosen since NP turned out to consist of TiO_2 and the O_3 concentration was sufficiently low at 23 $\pm$ 11 ppb to avoid any irritation during animal exposure. Data were collected at 5-min intervals over 2-h long TiO_2 aerosol production experiments. Production of amorphous versus crystalline TiO_2 NP was achieved without or with thermal heat treatment of the NP aerosol in a tube furnace downstream of the ^{85}Kr aerosol neutralizer, respectively.

Aerosol characterization

The aerosol was usually diluted and adjusted to a concentration of 3–6 $\times$ 10^6 NP cm^{-3} at a total flow of 10 L min^{-1} and was constant to within $\pm$20% over several hours per day (Fig. 4) and even for several consecutive days (data not shown). Mean mass concentrations determined by the weight of filter samples were about 60 μg m^{-3} (36 μg h^{-1}). The median mobility diameter determined by DMPS and the geometric standard deviation also remained

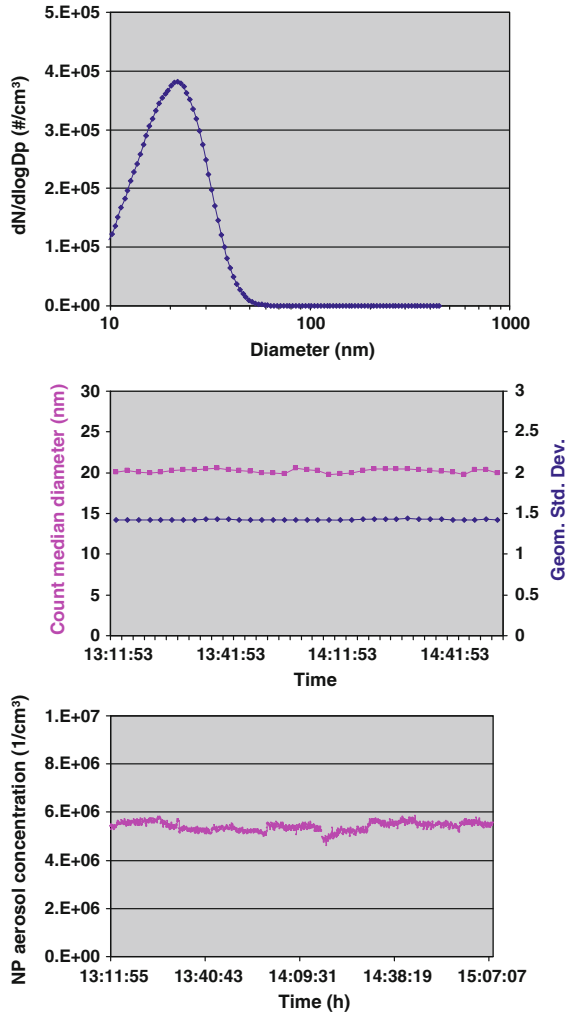

Fig. 4 Average TiO_2 NP aerosol size distribution (*left upper*) and concentration (*left lower*) during 1 h of generation; variation of the count median diameter and geometric standard deviation during 1 h of generation (*right upper*)

constant to within about $\pm$15 and $\pm$10%, respectively (Fig. 4). The median mobility diameter of the thermally untreated NP was about 20–25 nm, whereas that of the thermally treated NP was about 10% less, as shown in Fig. 5. Reproducibility of the aerosol generation was found be satisfactory as demonstrated during the intermittent daily aerosol production for the collection of TiO_2 powders for BET analysis (see "Methods" section).

When using ^{48}V radiolabeled electrodes, the specific ^{48}V activity of the aerosol was 1.5 MBq m^{-3}, and the specific ^{48}V activity per NP mass was

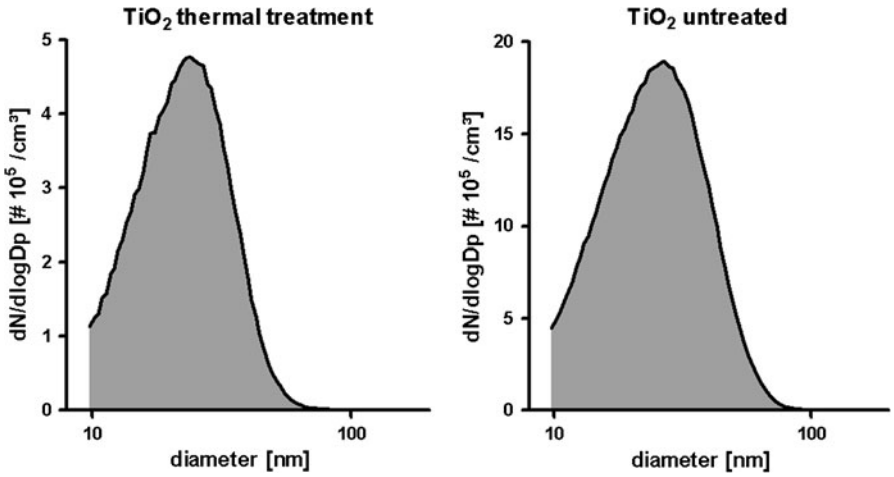

Fig. 5 Size distribution of TiO_2 NP aerosol with (*upper*) and without (*lower*) thermal after-treatment

27 MBq mg^{-1}. This corresponds to a ^{48}V activity of 1.7×10^{-7} Bq per single NP.

TiO_2 NP morphology

TEM analyses revealed that the as-generated (non heat-treated) particles consist of almost spherical primary particles of 2–5 nm in (geometric) diameter. The primary particles are linked into a chain-like agglomerate morphology with a variable length between about a ten and several tens of nanometers depending on the direction of measurement (Fig. 6, upper right). This is consistent with the observed median mobility diameter of 20–25 nm, since for loosely packed, fractal-like agglomerates as encountered here (fractal dimension is estimated to be about 1.5–2.0) the minimum and maximum length of an agglomerate is about 2–3 times smaller and larger than the corresponding mobility diameter, respectively (Baron and Willeke 2001). From high resolution imaging combined with diffraction measurements the agglomerated particles are found to have an amorphous structure (Fig. 6, lower right). Investigations of the particles sintered at 950 °C reveal a similar morphology as for the as-generated particles. Again the particles are found to have a chain-like agglomerate morphology consisting of almost spherical primary particles of a few nanometers, probably slightly more strongly agglomerated together (Fig. 6, upper left), which is in good agreement with the heat treatment studies of Seto et al. (1995). However, the structure of the individual agglomerated particles has transformed from amorphous to crystalline (Fig. 6, lower left). Comparing the as-generated particles with the heat-treated ones, it is clear that the sintering process modifies the internal structure of the particles but to a lesser extent affects their overall morphology. For such morphological changes, a higher temperature would have been necessary (Karlsson et al. 2005). The phase transformation of TiO_2 depends on surface energy which is directly related to the size of the NP (Gribb and Banfield 1997). Detailed studies on crystal phase transformation, both during synthesis and post treatment, have been conducted in earlier studies (Yang et al. 1996)—see also the "Discussion" section.

In addition, electron tomography allows the 3D characterization of TiO_2 NP collected from the aerosol. By acquiring a set of projection images at a range of angles, the particles can be analyzed throughout the whole stack volume. As shown in Fig. 7a–c, the TiO_2 NP adopt different morphologies in different planes of the image stack. In the 3D reconstruction (Fig. 7d), the NP appear unconnected to the *xy*-plane, i.e., the TEM grid. This is probably due to thickness fluctuations (up to 25 nm) of the formvar support film. Another structural feature seen in the tomograms is that of Bragg diffractions which induce scattering contrast in bright field TEM due to lattice plane orientation of crystalline areas. In the tomograms, they appear as contrast-rich areas with rapid contrast reduction upon slight angular tilting (Fig. 7a_1–a_3). Bragg reflections alter the contrast at each tilt image. This contrast variation is not usually preferred, though its effect on the final result decreases with the number of images taken (Takaoka et al. 2008). The TiO_2 NP agglomerates observed in

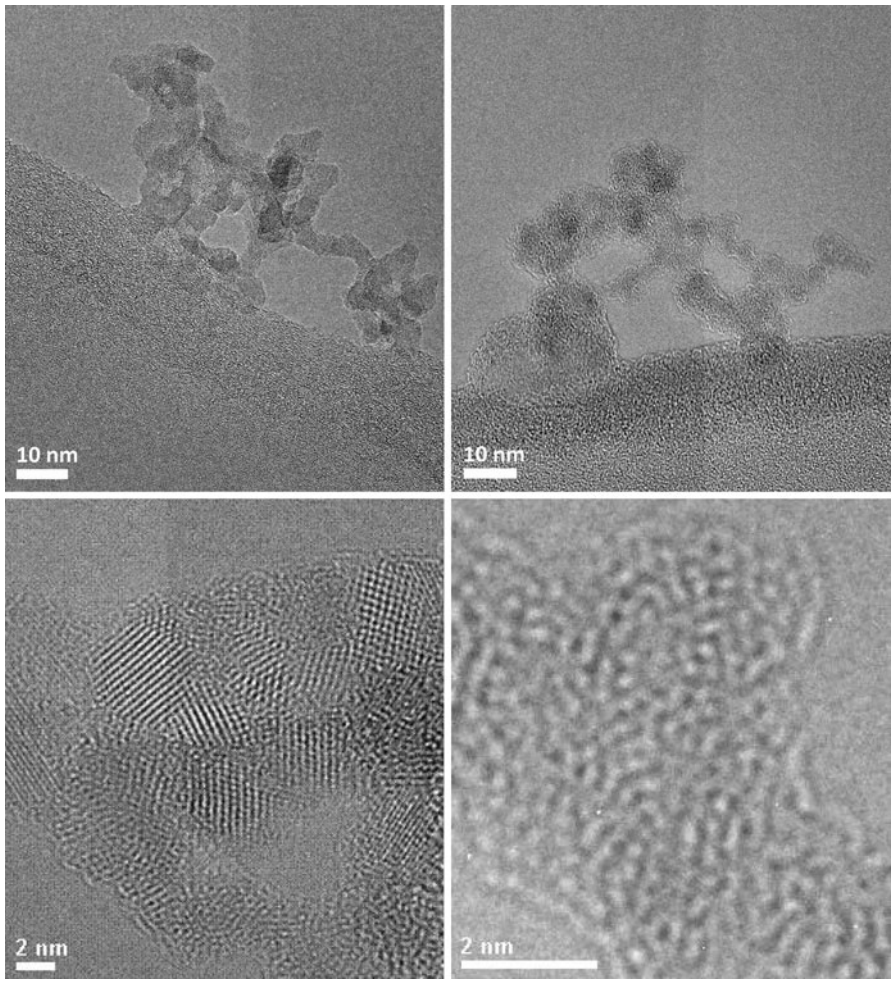

Fig. 6 TEM and HRTEM: *Left upper* thermally treated crystalline TiO_2. *Right upper* thermally untreated amorphous TiO_2 NP. *Left lower* thermally treated crystalline TiO_2 NP. *Right lower* thermally untreated amorphous TiO_2 NP

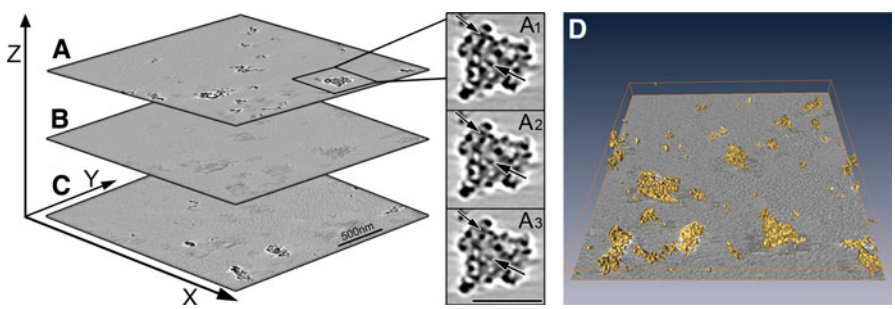

Fig. 7 TEM images, Bragg reflections and reconstructed electron tomogram of TiO_2 NP. The tilt series consisted of 64 images obtained between −40 and 40° tilt angle with an evenly spaced increment of 2°. The magnification was 80,000×. *Left* Topmost (**a**), middle (**b**) and lowest (**c**) image of the tomographic reconstruction. *Middle* Bragg diffractions (*arrows*) appear as contrast-rich areas with rapid contrast reduction upon slight angular tilting ($\mathbf{a}_1$–$\mathbf{a}_3$ consecutive images). *Right* 3D reconstruction of the TiO_2 NP (in gold) and the lowermost image of the electron tomogram

vivo and after sampling of the humidified aerosol (Kapp et al. 2004) have different structural organizations when compared to Fig. 6 (right) but they appear slightly more compact than the loosely arranged amorphous TiO_2 aerosol NP. This humidity-associated restructuring of agglomerated NP was

reported earlier (Weber et al. 1996). In electron tomography as well as in conventional TEM, an overall heterogeneous particle structure can be recognized which makes it more difficult to find NP in tissue samples. In this case, Bragg reflections provide additional information on the TiO_2 NP in electron tomography that helps to identify these NP in biological specimens.

Chemical analysis of TiO_2 NP

Both NP powders—heat-treated and non-heat-treated—collected for the BET measurements, were white in color. Regarding chemical composition, XEDS measurements confirm that the generated particles contain titanium and oxygen. Furthermore, results of quantification of XEDS for 10 and 16 measured particles, show, respectively, average atomic % compositions of 36/64 (Ti/O) and 36/64 (Ti/O) for the as-generated and the sintered particles. Given the accuracy limit of about ±2 atomic % for XEDS, these results confirm that the particles are composed of TiO_2. In addition, oxygen and titanium maps produced by EFTEM demonstrate that the oxygen and titanium are evenly distributed inside the particles, further confirming the TiO_2 composition.

TiO_2 NP crystallinity

The GAXRD pattern, taken at an incident angle of 1°, for the heat-treated TiO_2 NP deposited onto a silicon wafer is presented in Fig. 8, together with reference lines for anatase and rutile. The pattern clearly indicates that the main TiO_2 crystalline phase is anatase, with no clear evidence to confirm the presence of the rutile phase. Certain XRD peak positions appear slightly shifted to higher angles than those that would be expected for a perfect anatase structure, indicating a probable *c*-axis lattice parameter about 1.5% shorter than the reference value. There is also a broad feature to the high angle side of the anatase 101 peak, the origin of which is not clear, although it could be associated with particularly small nanocrystalline domains, or possibly crystalline-stacking faults. Point defects such as impurities, vacancies or interstitials could all be present in the NP structure. While the signal/noise ratio is not good enough for accurate peak deconvolution, the anatase XRD peaks appear to display both microstrain and significant crystallite size broadening. The microstrain would again be consistent with the presence of point defects, while the crystallite size can be roughly estimated to be 4–5 nm.

For the 15 mg TiO_2 NP powder sample, the crystal phase was confirmed to predominantly consist of anatase as shown in Fig. 9. The non-identified wide feature at about 30° is also seen in this sample. Peak width analysis using Scherrer's formula again indicates a crystallite size of 4–5 nm.

Specific surface area of TiO_2 NP

The measured surface area of the thermally treated anatase TiO_2 NP from BET measurement was found

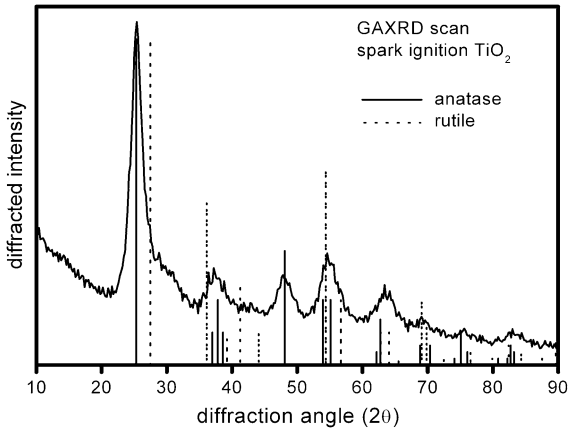

Fig. 8 XRD of a thermally treated TiO_2 NP sample on a silicon wafer

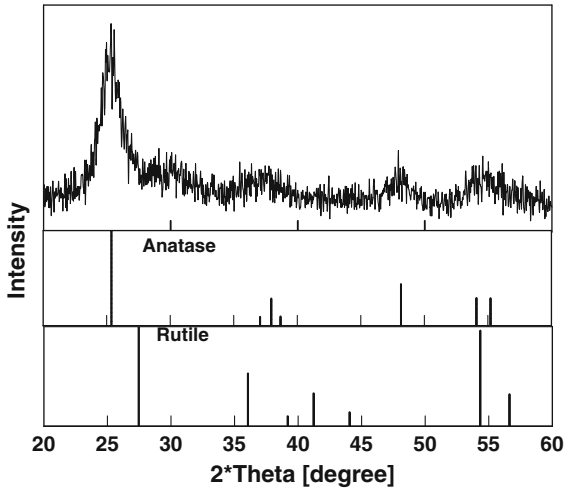

Fig. 9 XRD of a thermally treated TiO_2 NP powder sample

to be 270.7 m^2 g^{-1}, whereas it was 330 m^2 g^{-1} for thermally untreated amorphous TiO_2 NP. The decreased surface area for the thermally treated TiO_2 is likely due to the sintering of the NP, which reduces the surface area at the points where the individual primary particles bond together. This moderate decrease of the specific surface area is in very good agreement with Seto et al. (1995). The equivalent diameters obtained from theses surface area measurements were ~5 nm for the amorphous NP and ~6 nm for the heat-treated material, assuming all primary particles to be spherical and of the same geometric diameter. These results are totally consistent with the XRD crystallite size analysis.

In vitro leaching of the radiolabel ^{48}V from the TiO_2 NP

The in vitro dissolution tests of non-heat-treated ^{48}V-TiO_2 NP generated by spark ignition showed a considerable ^{48}V-loss of up to 25% after 24 h. In contrast, when the NP-aerosols had been heat treated at 950 °C in the tube furnace immediately after their generation, the leached ^{48}V-fraction of the thermally treated TiO_2 NP amounted to less than 2% of the total activity within 24 h, and remained negligible thereafter. Obviously, in the non-heat-treated state, the ^{48}V radiolabel is only loosely bonded or trapped in the amorphous NP structure. The observed decrease of ^{48}V leaching indicates an increased integration of the radiolabel into the crystalline TiO_2 lattice formed during heat treatment.

Distribution and clearance of inhaled TiO_2 NP

The establishment of the morphology and the section profiles of the aerosol particles as shown in Fig. 10, allowed the morphological identification of TiO_2 in ultrathin tissue sections. However, elemental microanalysis by EFTEM is additionally required to confirm the elemental composition of the NP, as there are other objects in the tissue that resemble the aerosol particles. As shown in Fig. 11, elemental (titanium) mapping achieved with the three-window methods reveals a strong signal and is highly suitable for the identification of the TiO_2 NP in tissue.

So far, our inhalation studies with TiO_2 NP in rats and mice showed that the majority of these NP remain on the luminal side of the air spaces (Geiser et al. 2005). These ultrafines may also penetrate the epithelial barrier and then distribute rapidly in the lung tissue. At low concentration, inhaled TiO_2 NP do not agglomerate and do not evoke inflammatory responses by influx of neutrophils. Inhaled TiO_2 NP are inefficiently phagocytosed by lung surface macrophages and are found in large phagolysosomes containing other material like surfactant (Geiser et al. 2008; Geiser and Kreyling 2010). In conclusion, these studies give strong evidence for prolonged lung-retention of inhaled TiO_2 NP, due to particle penetration into the lung tissue and inefficient macrophage clearance. There is a potential, however, considered to be small, for systemic translocation of TiO_2 NP into secondary target organs. A comparison of the size of TiO_2 NP estimated by measuring the (geometric) diameters of the particle profiles in ultrathin sections of lung tissue and macrophages, and that assessed by a differential mobility particle sizer in the aerosol (equivalent mobility diameter) gave no evidence for particle agglomeration (Geiser et al. 2005).

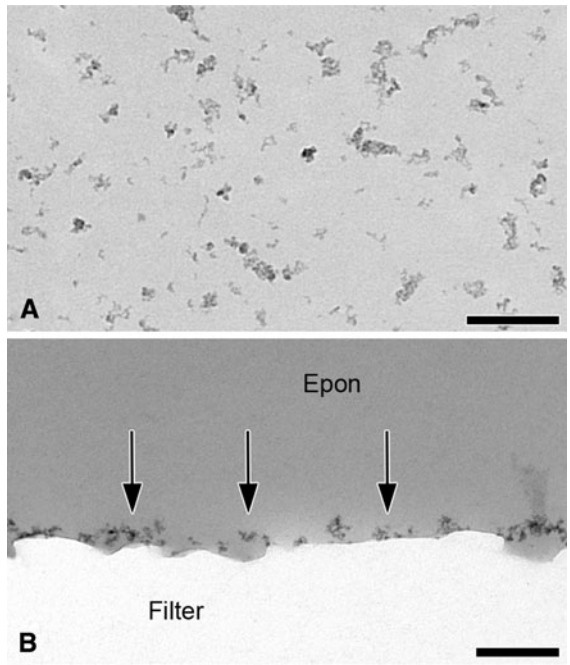

Fig. 10 Morphology and section profiles of TiO_2 NP in conventional TEM. **a** Area profiles of TiO_2 NP collected from the aerosol on a formvar-coated 600-mesh hexagonal copper grid. **b** TEM micrograph of particle profiles in ultrathin section of epon-embedded TiO_2 aerosol sampled on filters. *Scale bars* 200 nm

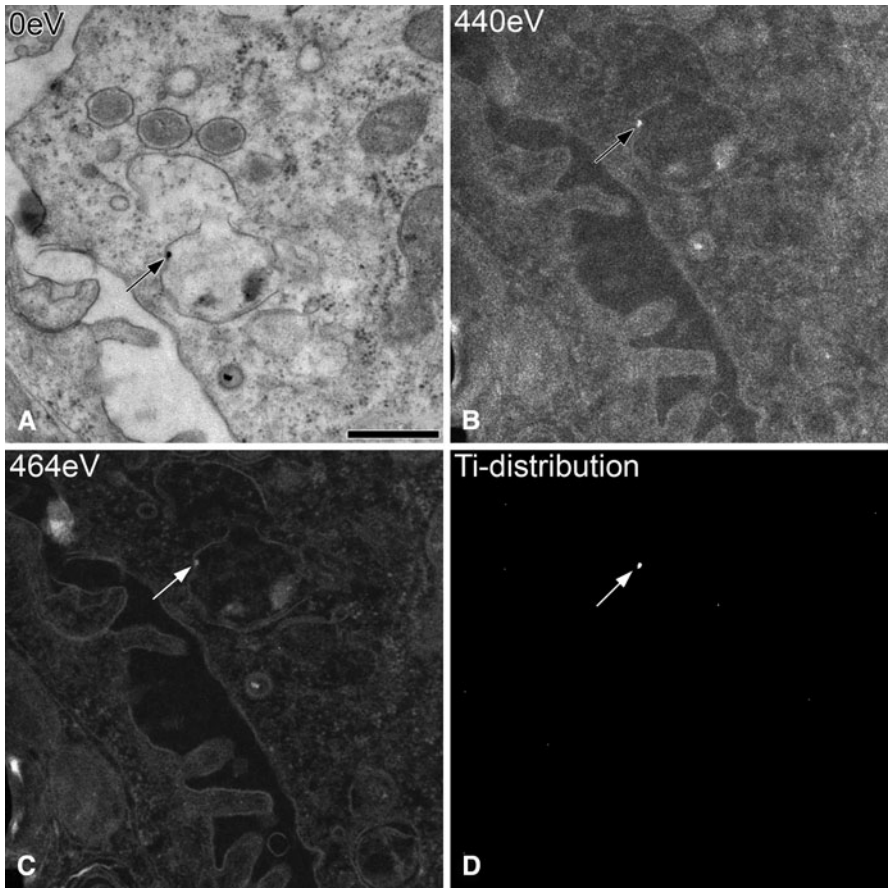

Fig. 11 Elemental microanalysis of TiO_2 NP in lung tissue. **a** ESI (three-window method), demonstrates that the NP (*arrow*) consists of titanium. Three images are taken: two below the element-specific edge to extrapolate (**a**) background image (390 eV, not shown and 440 eV, **b**), and one image within the maximum (**c**, 464 eV) of the element specific signal. The net titanium signal in (**d**) is calculated by subtraction of the extrapolated background image from the titanium-specific signal. The obtained image reflects the titanium distribution in white pixels. The 0 eV image demonstrates the structural details; it is slightly shifted as compared to the images used for elemental microanalysis. Reprinted from Geiser and Kreyling (2010). *Scale bar* 500 nm

Discussion

The described spark ignition generator is capable of providing approximately 20 nm TiO_2 NP aerosols at high particle number concentration of 3–6 $\times$ 10^6 cm^{-3} with a lognormal size distribution (median mobility diameter 20–25 nm and a geometric standard deviation of 1.6); mass concentration was about 60 $\mu g\ m^{-3}$. This number concentration is the upper limit above which diffusional coagulation is likely to modify the size distribution and number concentration within several seconds. The aerosol production was stable over several hours and for several consecutive days. The freshly produced NP aerosols may be used within 5–10 s for inhalation experiments with rodents to specifically study deposition of these very small particles in the respiratory tract and their interactions with lung tissues. It can be noted that such small-sized NP aerosols for inhalation can usually not be achieved when starting from NP powders since the powder cannot be completely dispersed and the particles remain in submicrometer-sized agglomerates/aggregates (Ma-Hock et al. 2007). Hence, the spark ignition methodology allows biomedical and toxicological studies focused on the interactions and effects of the smallest NP with respiratory tract tissues and subsequently, via blood circulation with tissues of secondary organs. This is a field which is largely unknown despite the fact that the increasing use of new types of engineered NP should imply risk assessments on the safety of these particles.

NP were characterized very thoroughly for their aerosol characteristics and also for their physico-chemical properties. Their stoichiometric composition was TiO_2. Morphologically they consisted of primary particles with 2–5-nm geometric diameter forming chain agglomerates/aggregates of 20–25 nm in diameter as determined by electron microscopy and electrical mobility sizing. This agglomerated structure is consistent with their relatively large specific surface area of about 330 $m^2\ g^{-1}$ (for the non-heat-treated NP). In the spark chamber, TiO_2 particles of exclusively amorphous structures were

produced. The amorphous chain agglomerates/aggregates were transformed by 950 °C heat treatment into pure anatase crystallites using a down-stream tube furnace but maintaining their chain agglomerate/aggregate structure as shown by HRTEM, which is in very good agreement to Seto et al. (1995). As a result, their BET-specific surface area was only slightly reduced to 270 $m^2\ g^{-1}$. Both forms of NP—either amorphous or crystalline—were available for toxicological studies. The phase transformation of TiO_2 depends on surface energy which is directly related to the size of the NP (Gribb and Banfield 1997). The anatase phase of the TiO_2 is thermodynamically more stable for size below 11 nm, whereas rutile is the most stable for sizes greater than 35 nm (Zhang and Banfield 2000). The critical size at which anatase starts to transform to rutile is around 14 nm. In this study, the primary particle sizes were less than 10 nm so the anatase phase alone was observed after heat treatment. Detailed studies on crystal phase transformation, both during synthesis and post treatment, have been conducted in earlier studies (Yang et al. 1996). Point defects and interstitial atoms in the crystalline lattice are mediators of solid-state diffusion in materials and control the crystal phase of the material, and thus may affect the biological activities. Some of our previous studies have also elucidated the role of surface defects on formation of ROS (Jiang et al. 2008). However, we cannot exclude the possibility that different NP morphologies as well as NP surface defects may affect biodistribution (the main focus of our inhalation studies) as well as the formation of ROS.

For NP labeling, proton irradiation of the tip of the titanium electrodes in a cyclotron caused a nuclear reaction by which ^{48}V atoms were formed within the lattice of the tip of the electrodes. During spark ignition ^{48}V was evaporated together with Ti atoms from the surface of the electrode and condensed with the primary TiO_2 particles. The ^{48}V-TiO_2 NP aerosol yielded a specific ^{48}V activity of 1.5 MBq m^{-3} and 27 MBq mg^{-1} NP mass. The specific ^{48}V radioactivity decreases rapidly after erosion of the first few milligram of Ti of the Ti electrodes which results in loss of ^{48}V activity of the NP aerosol. However, at the aerosol mass concentration of about 60 μg m^{-3} produced at a total aerosol flow rate of 10 L min^{-1}, 30 h of continuous aerosol operation are required to erode each milligram; so major changes would only occur after more than 30 rodent exposures lasting 1 h. This needs to be borne in mind but is not normally anticipated since the physical decay time of 16 days of ^{48}V, together with the laboratory capacity for radioanalytical analysis, does not allow more than 3–5 rodent exposures with one set of irradiated electrodes. Some variation in the specific ^{48}V radioactivity in the NP will occur according to the slightly non-uniform ^{48}V activity distribution with increasing depth of the electrodes, and also due to radioactive decay over time. The variation over a typical inhalation time of 1 h will be minimal. With regard to longer-term variations, both effects can be corrected for by collection of all excretions and complete accounting of all activities in the various organs as we do in our quantitative biokinetics studies (Semmler-Behnke et al. 2008; Geiser and Kreyling 2010). Long inhalations over several hours, or sequential inhalations on the same animal at widely differing times, are not generally performed.

To firmly bind the ^{48}V radiolabel within the lattice of the primary TiO_2 particles, heat treatment at 950 °C in the tube furnace was required. The leached fraction of the ^{48}V radiolabel from the TiO_2 NP in distilled water was <2% of the ^{48}V radioactivity within 24 h and remained negligible thereafter. These in vitro tests in distilled water provide only a first estimate on the leachability of the ^{48}V radiolabel. For a full analysis of in vivo leaching, comparison of biokinetic results of inhaled ^{48}V TiO_2 NP with those of soluble ^{48}V radiolabel alone is necessary: from the metabolic differences observed in these studies, the in vivo leaching of the ^{48}V radiolabel off the NP can be quantified as we have shown previously for inhaled ^{192}Ir NP aerosols (Kreyling et al. 2002; Semmler et al. 2004).

Since only very low specific radioactivity of the ^{48}V TiO_2 NP is required for their quantification in toxicological studies, the ratio between ^{48}V and Ti in the NP is 5×10^{-6}. Hence, most of the 2–5 nm primary particles do not contain any ^{48}V atom and, on average, there is less than one ^{48}V isotope per 20 nm agglomerate/aggregate.

It is worthy to note that the TiO_2 NP aerosol generation method used by Seto et al. (1995) is more elaborate while our spark ignition methodology is simpler and more robust and provides a stable, high concentration aerosol output over several hours; furthermore, it also includes the option of easy

radiolabeling. Alternative methods for the generation of TiO_2 NP aerosols that provide higher mass output rates are less suitable for our rodent inhalation studies because of larger particle size due to rapid coagulation and higher flow rates which are not required. They are also clearly less suitable for use with radiolabeled NP, due to the need for increased amounts of radioactive material. Our technique provides the highest number concentration theoretically possible ($3–6 \times 10^6$ cm^{-3}) limited only by unavoidable rapid coagulation.

In our previous study, the size distribution of amorphous TiO_2 NP aerosol with a count median mobility diameter of 22 nm and a GSD of 1.7 (measured by electrical mobility sizing) was compared with the size distribution after deposition in the lungs of rats (measured by EFTEM) showing a count median geometric diameter of 29 nm and a similar GSD of 1.7 (Kapp et al. 2004). Size measurements of NP profiles in ultrathin tissue sections and aerosol electrical mobility analysis are very different methodologies, and the size comparison of the SMPS and TEManalyses is only valid for compact particles. Yet, the agreement of both distributions is surprisingly good. As a result, these data do not support speculations about appreciable disintegration of the deposited TiO_2 NP in lung tissue.

Summary

Spark ignition technology has been used for reproducible production of highly concentrated ($3–6 \times 10^6$ cm^{-3}; ~60 μg m^{-3}, 36 μg h^{-1}) polydispersed TiO_2 NP aerosols which proved to be constant over several hours in terms of their count median mobility diameter, geometric standard deviation and number concentration. Either crystalline pure anatase TiO_2 NP or amorphous TiO_2 NP was produced, respectively, with or without 950 °C heat treatment of the aerosol downstream of the spark ignition generator. Both crystalline and amorphous 20–25 nm (median mobility diameter) TiO_2 NP were chain agglomerates/aggregates consisting of primary particles with a geometric diameter of about 5 nm. The TiO_2 NP were extensively characterized in terms of their chemical composition, physical structure, morphology and specific surface area. Disintegration of the deposited TiO_2 NP in lung tissue was not detectable. In addition, TiO_2 NP were radiolabeled with ^{48}V by proton irradiation of the titanium electrodes of the spark generator, and the radiolabel leaching rate in water attained within the first day was about 1%.

Acknowledgments This study was partially funded by HMGU: EU FP7 projects—NeuroNano (NMP4-SL-2008-214547), ENPRA (NMP4-SL-2009-228789), and InLiveTox (NMP4-SL-2009-228625); UBA-Germany project: Z6 (55 410-31/3); UBern: Swiss National Science Foundation project (310030-120763); and Lund: the Nanometer Structure Consortium at Lund University. The authors express their sincere gratitude to Jürgen Daul and Dr. Achim Kleinrahm, ZAG Zyklotron AG, Karlsruhe, Germany, for their help in proton irradiation of the titanium electrodes.

References

Almquist CB, Sahle-Demessie E, Enriquez J, Biswas P (2003) The photocatalytic oxidation of low concentration MTBE on titanium dioxide from groundwater in a falling film reactor. Environ Prog 22(1):14–24

Barnard AS (2010) One-to-one comparison of sunscreen efficacy, aesthetics and potential nanotoxicity. Nat Nanotechnol 5(4):271–274

Baron PA, Willeke K (2001) Aerosol measurement. Wiley Interscience, New York

Baumeister W (2002) Electron tomography: towards visualizing the molecular organization of the cytoplasm. Curr Opin Struct Biol 12:679–684

Boffetta P, Soutar A, Cherrie JW, Granath F, Andersen A, Anttila A, Blettner M, Gaborieau V, Klug SJ, Langard S, Luce D, Merletti F, Miller B, Mirabelli D, Pukkala E, Adami HO, Weiderpass E (2004) Mortality among workers employed in the titanium dioxide production industry in Europe. Cancer Causes Control 15:697–706

Borm PJ, Schins RP, Albrecht C (2004) Inhaled particles and lung cancer, part B: paradigms and risk assessment. Int J Cancer 110:3–14

Chen X, Mao SS (2007) Titanium dioxide nanomaterials: synthesis, properties, modifications, and applications. Chem Rev 107:2891–2959

Dankovic D, Kuempel E, Wheeler M (2007) An approach to risk assessment for TiO_2. Inhal Toxicol 19(Suppl 1): 205–212

Fryzek JP, Chadda B, Marano D, White K, Schweitzer S, McLaughlin JK, Blot WJ (2003) A cohort mortality study among titanium dioxide manufacturing workers in the United States. J Occup Environ Med 45:400–409

Geiser M, Kreyling WG (2010) Deposition and biokinetics of inhaled nanoparticles. Particle Fibre Toxicol 7:2. doi: 10.1186/1743-8977-7-2

Geiser M, Rothen-Rutishauser B, Kapp N, Schürch S, Kreyling W, Schulz H, Semmler M, Im Hof V, Heyder J, Gehr P (2005) Ultrafine particles cross cellular membranes by non-phagocytic mechanisms in lungs and in cultured cells. Environ Health Perspect 113:1555–1560

Geiser M, Casaulta M, Kupferschmid B, Schulz H, Semmler-Behnke M, Kreyling W (2008) The role of macrophages in the clearance of inhaled ultrafine titanium dioxide particles. Am J Respir Cell Mol Biol 38:371–376

Gribb AA, Banfield JF (1997) Particle size effects on transformation kinetics and phase stability in nanocrystalline TiO_2. Am Mineral 82:717–728

Heinrich U, Fuhst R, Rittinghausen S, Creutzenberg O, Bellmann B, Koch W, Levsen K (1995) Chronic inhalation exposure of Wistar rats and two different strains of mice to diesel engine exhaust, carbon black, and titanium dioxide. Inhal Toxicol 7:533–556

Jani PU, McCarthy DE, Florence AT (1994) Titanium dioxide (rutile) particle uptake from the rat GI tract and translocation to systemic organs after oral administration. Int J Pharm 105:157–168

Jiang J, Oberdörster G, Elder A, Gelein R, Mercer P, Biswas P (2008) Does nanoparticle activity depend upon size and crystal phase? Nanotoxicology 2(1):33–42

Kapp N, Kreyling W, Schulz H, Im Hof V, Semmler M, Gehr P, Geiser M (2004) Identification of inhaled ultrafine titanium oxide particles by analytical electron microscopy in rat lungs. Microsc Res Tech 63:298–305

Karlsson MNA, Deppert K, Karlsson LS, Magnusson MH, Malm J-O, Srinivasan NS (2005) Compaction of agglomerates of aerosol nanoparticles: a compilation of experimental data. J Nanopart Res 7:43–49. doi:10.1007/s11051-004-7218-3

Kreyling WG, Semmler M, Erbe F, Mayer P, Takenaka S, Oberdörster G, Ziesenis A (2002) Translocation of ultrafine insoluble iridium particles from lung epithelium to extrapulmonary organs is size dependent but very low. J Toxicol Environ Health 65(20):1513–1530

Kreyling WG, Semmler-Behnke M, Seitz J, Scymczak W, Wenk A, Mayer P, Oberdörster G (2009) Size dependence of the translocation of inhaled iridium and carbon nanoparticle aggregates from the lung of rats to the blood and secondary target organs. Inhal Toxicol 21(S1):55–60

Lekki J, Stachura Z, Dabros W, Stachura J, Menzel F, Reinert T, Butz T, Pallon J, Gontier E, Ynsa MD, Moretto P, Kertesz Z, Szikszai Z, Kiss AZ (2007) On the follicular pathway of percutaneous uptake of nanoparticles: ion microscopy and autoradiography studies. Nucl Instrum Methods Phys Res B 260:174–177

Li Q, Mahendra S, Lyon DY, Brunet L, Liga MV, Li D, Alvarez PJJ (2008) Antimicrobial nanomaterials for water disinfection and microbial control: potential applications and implications. Water Res 42:4591–4602

Lomer MC, Hutchinson C, Volkert S, Greenfield SM, Catterall A, Thompson RP, Powell JJ (2004) Dietary sources of inorganic microparticles and their intake in healthy subjects and patients with Crohn's disease. Br J Nutr 92(6):947–955

Ma-Hock L, Gamer AO, Landsiedel R, Leibold E, Frechen T, Sens B et al (2007) Generation and characterization of test atmospheres with nanomaterials. Inhal Toxicol 19(10):833–848

Nohynek GJ, Dufour EK, Roberts MS (2008) Nanotechnology, cosmetics and the skin: is there a health risk? Skin Pharmacol Physiol 21:136–149

Rehman S, Ullah R, Butt AM, Gohar ND (2009) Strategies of making TiO_2 and ZnO visible light active. J Hazard Mater 170:560–569

Semmler M, Seitz J, Erbe F, Mayer P, Heyder J, Oberdörster G, Kreyling WG (2004) Long-term clearance kinetics of inhaled ultrafine insoluble iridium particles from the rat lung, including transient translocation into secondary organs. Inhal Toxicol 16(6–7):453–459

Semmler-Behnke M, Kreyling W, Lipka J, Fertsch S, Wenk A, Takenaka S, Schmid G, Brandau W (2008) Biodistribution of 1.4- and 18-nm gold particles in rats. Small 4(12):2108–2111

Seto T, Shimada M, Okuyama K (1995) Evaluation of sintering of nanometer-sized titania using aerosol method. Aerosol Sci Technol 23(2):183–200

Takaoka A, Hasegawa T, Yoshida K, Mori H (2008) Microscopic tomography with ultra-HVEM and applications. Ultramicroscopy 108:230–238

Weber AP, Baltensperger U, Gaggeler HW, Schmidt-Ott A (1996) In situ characterization and structure modification of agglomerated aerosol particles. J Aerosol Sci 27(6):915–929

Yang GM, Zhuang H, Biswas P (1996) Characterization and sinterability of nanophase titania particles processed in flame reactors. NanoStruct Mater 7(6):675–689

Zhang H, Banfield JF (2000) Understanding polymorphic phase transformation behavior during growth of nanocrystalline aggregates: Insights from TiO_2. J Phys Chem B 104:3481–3487

Zhang H, Finnegan M, Banfield JF (2001) Preparing single-phase nanocrystalline anatase from amorphous titania with particle sizes tailored by temperature. Nano Lett 1(2):81–85